WITH FALSE FRIENDS LIKE THESE, WHO CAN HAVE SELF-KNOWLEDGE?

Anonymous authors
Paper under double-blind review

ABSTRACT

Adversarial examples arise from excessive sensitivity of a model. Commonly studied adversarial examples are malicious inputs, crafted by an *adversary* from correctly classified examples, to induce misclassification. This paper studies an intriguing, yet far overlooked consequence of the excessive sensitivity, that is, a misclassified example can be easily perturbed to help the model to produce correct output. Such perturbed examples look harmless, but actually can be maliciously utilized by a *false friend* to make the model self-satisfied. Thus we name them *hypocritical examples*. With false friends like these, a poorly performed model could behave like a state-of-the-art one. Once a deployer trusts the hypocritical performance and uses the "well-performed" model in real-world applications, potential security concerns appear even in benign environments. In this paper, we formalize the *hypocritical risk* for the first time and propose a defense method specialized for hypocritical examples by minimizing the tradeoff between natural risk and an upper bound of hypocritical risk. Moreover, our theoretical analysis reveals connections between adversarial risk and hypocritical risk. Extensive experiments verify the theoretical results and the effectiveness of our proposed methods.

1 INTRODUCTION

Deep neural networks (DNNs) have achieved breakthroughs in a variety of challenging problems such as image understanding (Krizhevsky et al., 2012), speech recognition (Graves et al., 2013), and automatic game playing (Mnih et al., 2015). Despite these remarkable successes, their pervasive failures in adversarial settings, the phenomenon of *adversarial examples* (Biggio et al., 2013; Szegedy et al., 2014), have attracted significant attention in recent years (Athalye et al., 2018; Carlini et al., 2019; Tramer et al., 2020). Such *small* perturbations on inputs crafted by adversaries are capable of causing well-trained models to make *big* mistakes, which indicates that there is still a large gap between machine and human perception, thus posing potential security concerns for practical machine learning applications (Kurakin et al., 2016; Qin et al., 2019; Wu et al., 2020b).

An adversarial example is "an input to a machine learning model that is intentionally designed by an attacker to fool the model into producing an incorrect output" (Goodfellow & Papernot, 2017). Following the definition of adversarial examples on classification problems (Goodfellow et al., 2015; Papernot et al., 2016; Elsayed et al., 2018; Carlini et al., 2019; Zhang et al., 2019; Wang et al., 2020b; Zhang et al., 2020; Tramèr et al., 2020), given a DNN classifier f and a *correctly* classified example $\boldsymbol{x}$ with class label y (i.e., $f(\boldsymbol{x}) = y$), an adversarial example $\boldsymbol{x}_{\mathsf{adv}}$ is generated by perturbing $\boldsymbol{x}$ such that $f(\boldsymbol{x}_{\mathsf{adv}}) \neq y$ and $\boldsymbol{x}_{\mathsf{adv}} \in \mathcal{B}_\epsilon(\boldsymbol{x})$. The neighborhood $\mathcal{B}_\epsilon(\boldsymbol{x})$ denotes the set of points within a fixed distance $\epsilon > 0$ of $\boldsymbol{x}$, as measured by some metric (e.g., the l_p distance), so that $\boldsymbol{x}_{\mathsf{adv}}$ is visually the "same" for human observers. Then, an imperfection of the classifier is highlighted by $\mathcal{G}_{\mathsf{adv}} = \mathrm{Acc}(\mathcal{D}) - \mathrm{Acc}(\mathcal{A})$, the performance gap between the accuracy (denoted by $\mathrm{Acc}(\cdot)$) evaluated on clean set sampled from data distribution $\mathcal{D}$ and adversarially perturbed set $\mathcal{A}$.

An adversary could construct such a perturbed set $\mathcal{A}$ that looks no different from $\mathcal{D}$ but can severely degrade the performance of even state-of-the-art DNN models. From direct attacks in the digital space (Goodfellow et al., 2015; Carlini & Wagner, 2017) to robust attacks in the physical world (Kurakin et al., 2016; Xu et al., 2020), from toy classification problems (Chen et al., 2020; Dobriban et al., 2020) to complicated perception tasks (Zhang & Wang, 2019; Wang et al., 2020a), from the high dimensional nature of the input space (Goodfellow et al., 2015; Gilmer et al., 2018) to the

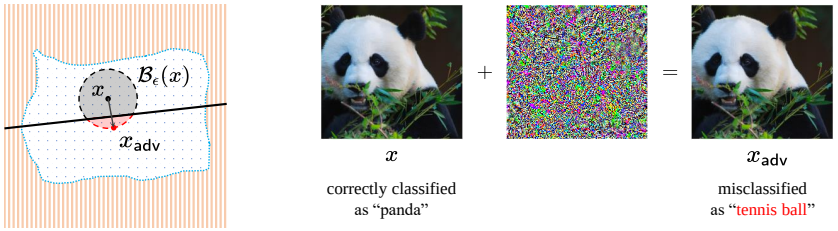

(a) Illustration of adversarial examples

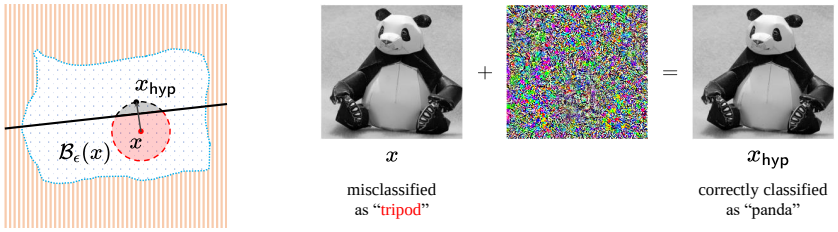

(b) Illustration of hypocritical examples

Figure 1: Comparison between adversarial examples and hypocritical examples. **Left**: Conceptual diagrams for the generation of an adversarial example $\boldsymbol{x}_{\mathsf{adv}}$ and a hypocritical example $\boldsymbol{x}_{\mathsf{hyp}}$. The input space is (ground-truth) classified into the orange lined region (e.g., class "not panda"), and the blue dotted region (e.g., class "panda"). The black solid line is the decision boundary of a non-robust model, which classifies the region above the boundary as "panda" and the region below the boundary as "not panda". Red shadow and black shadow in the ball $\mathcal{B}_\epsilon(\boldsymbol{x})$ denote that the points in there are misclassified and correctly classified, respectively. As we can see, $\boldsymbol{x}_{\mathsf{adv}}$ or $\boldsymbol{x}_{\mathsf{hyp}}$ can be easily found by perturbing a correctly classified $\boldsymbol{x}$ or a misclassified $\boldsymbol{x}$ across the model's decision boundary. **Right**: A demonstration of adversarial examples and hypocritical examples on real data. Here we choose ResNet50 (He et al., 2016a) trained on ImageNet (Russakovsky et al., 2015) as the victim model. In (a) the correctly classified "panda" can be stealthily perturbed to be misclassified as "tennis ball". In (b) the "panda" (misclassified as "tripod") can be stealthily perturbed to be correctly classified. Perturbations are rescaled for display.

framework of (non)-robust features (Jetley et al., 2018; Ilyas et al., 2019), many efforts have been devoted to understanding and mitigating the risk raised by adversarial examples, thus closing the gap $\mathcal{G}_{\mathsf{adv}}$. Previous works mainly concern the adversarial risk on correctly classified examples. However, they typically neglect a risk on misclassified examples themselves which will be formalized in this work.

In this paper, we first investigate an intriguing, yet far overlooked phenomenon, where given a DNN classifier f and a *misclassified* example $\boldsymbol{x}$ with class label y (i.e., $f(\boldsymbol{x}) \neq y$), we can easily perturb $\boldsymbol{x}$ to $\boldsymbol{x}_{\mathsf{hyp}}$ such that $f(\boldsymbol{x}_{\mathsf{hyp}}) = y$ and $\boldsymbol{x}_{\mathsf{hyp}} \in \mathcal{B}_\epsilon(\boldsymbol{x})$. Such an example $\boldsymbol{x}_{\mathsf{hyp}}$ looks harmless, but actually can be maliciously utilized by a *false friend* to fool a model to be self-satisfied. Thus we name them *hypocritical examples* (see Figure 1 for a comparison with adversarial examples) [1] .

Adversarial examples and hypocritical examples are two sides of the same coin. On the one side, a well-performed but sensitive model becomes unreliable in the existence of adversaries. On the other side, a poorly performed but sensitive model behaves well with the help of friends.

With friends like these, a naturally trained suboptimal model could have state-of-the-art performance, and even more, a randomly initialized model could behave like a well-trained one (see Section 2.1). If those friends are faithful, the improvement of performance is promising. In practice, a private high-performance model can be used as a surrogate of the true friend to consistently

[1] There are a few papers (e.g., Wang et al. (2017); Weng et al. (2018)) considering x^* an adversarial example as long as it is classified differently from x, thus they treat x_{adv} and x_{hyp} indiscriminately, while we differentiate x_{hyp} from x_{adv} due to their different intrinsic meanings. To the best of our knowledge, this is the first attempt to formalize the realistic risk raised by hypocritical examples.

help a weak model without exposing training data and model weights for the purpose of privacy protection and knowledge transfer (Abadi et al., 2016; Papernot et al., 2017a). However, if such so-called friends are unfaithful, the improvement becomes hypocritical and the excessive sensitivity of a model becomes undesirable. This paper focuses on the latter case.

In such a case, if the examples used to evaluate a model are falsified by a false friend, the model will manifest like a perfect one (on hypocritical examples), but it actually may not be well performed even on clean examples, not to mention adversarial examples. Thus a new imperfection of the classifier can be found in $\mathcal{G}_{\mathsf{hyp}} = \mathrm{Acc}(\mathcal{F}) - \mathrm{Acc}(\mathcal{D})$, the performance gap between the accuracy evaluated on clean set sampled from $\mathcal{D}$ and hypocritically perturbed set $\mathcal{F}$. Still, $\mathcal{F}$ looks no different from $\mathcal{D}$ but can stealthily upgrade the performance. Once a deployer trusts the hypocritical performance carefully designed by a false friend and uses the "well-performed" model in real-world applications, potential security concerns appear even in benign environments. Thus we need methods to defend our models from false friends, that is, making our models have self-knowledge.

We propose a defense method by improving model robustness against hypocritical perturbations. Specifically, we formalize the *hypocritical risk* and minimize it via a differentiable surrogate loss (Section 3). Experimentally, we verify the effectiveness of our proposed attack (Section 2) and defense (Section 4). Further, we study the transferability of hypocritical examples across models trained with various methods (Section 5). Finally, we conclude our paper by discussing and summarizing our results (Section 6 and Section 7). Our main contributions are:

- We give a formal definition of hypocritical examples. We demonstrate the unreliability of standard evaluation process in the existence of false friends and show the potential security risk on the deployment of a model with high hypocritical performance.
- We formalize the hypocritical risk and analyze its relation with natural risk and adversarial risk. We propose the first defense method specialized for hypocritical examples by minimizing the tradeoff between the natural risk and an upper bound of hypocritical risk.
- Extensive experiments verify the effectiveness of our proposed methods. We also examine the transferability of hypocritical examples. We show that the transferability is not always desired by false friends, which depends on their purpose.

2 False Friends and Adversaries

Better an open enemy than a false friend! Only by being aware of the potential risk of the false friend can we prevent it. In this section, we expose a kind of false friends, who are capable of manipulating model performance stealthily during the evaluation process, thus making the evaluation results unreliable.

We consider a classification task with data $(\boldsymbol{x}, y) \in \mathbb{R}^d \times \{1, \ldots, C\}$ from a distribution $\mathcal{D}$. Denote by $f : \mathbb{R}^d \to \{1, ..., C\}$ the classifier which predicts the class of an input example $\boldsymbol{x}$: $f(\boldsymbol{x}) = \arg\max_k p_k(\boldsymbol{x})$, where $p_k(\boldsymbol{x})$ is the kth component of $p(\boldsymbol{x}) : \mathbb{R}^d \to \Delta^C$ (e.g., the output after softmax activation), in which $\Delta^C = \{\boldsymbol{u} \in \mathbb{R}^C \mid \mathbf{1}^T \boldsymbol{u} = 1, \boldsymbol{u} \geq \mathbf{0}\}$ is the probabilistic simplex.

Adversarial examples are *malicious* inputs crafted by an adversary to induce misclassification. We first give the commonly accepted definition of adversarial examples as follows:

Definition 1 (Adversarial Examples)**.** *Given a classifier f and a correctly classified input $(\boldsymbol{x}, y) \sim \mathcal{D}$ (i.e., $f(\boldsymbol{x}) = y$), an ϵ-bounded adversarial example is an input $\boldsymbol{x}^* \in \mathbb{R}^d$ such that:*

$$f(\boldsymbol{x}^*) \neq y \quad \textit{and} \quad \boldsymbol{x}^* \in \mathcal{B}_\epsilon(\boldsymbol{x}).$$

The assumption underlying this definition is that inputs satisfying $\boldsymbol{x}^* \in \mathcal{B}_\epsilon(\boldsymbol{x})$ preserve the label y of the original input $\boldsymbol{x}$. The reason for the existence of adversarial examples is that a model is overly sensitive to non-semantic changes. Next, we formalize a complementary phenomena to adversarial examples, called hypocritical examples. Hypocritical examples are *malicious* inputs crafted by a false friend to stealthily correct the prediction of a model:

Definition 2 (Hypocritical Examples)**.** *Given a classifier f and a misclassified input $(\boldsymbol{x}, y) \sim \mathcal{D}$ (i.e., $f(\boldsymbol{x}) \neq y$), an ϵ-bounded hypocritical example is an input $\boldsymbol{x}^* \in \mathbb{R}^d$ such that:*

$$f(\boldsymbol{x}^*) = y \quad \textit{and} \quad \boldsymbol{x}^* \in \mathcal{B}_\epsilon(\boldsymbol{x}).$$

The same as adversarial examples, hypocritical examples are bounded to preserve the label of the original input, and are another consequence that arises from excessive sensitivity of a classifier.

As a false friend, a hypocritical example can be generated from a misclassified example by maximizing

$$\max_{\boldsymbol{x}' \in \mathcal{B}_\epsilon(\boldsymbol{x})} \mathbb{1}(f(\boldsymbol{x}') = y), \tag{1}$$

which is equivalent to minimizing

$$\min_{\boldsymbol{x}' \in \mathcal{B}_\epsilon(\boldsymbol{x})} \mathbb{1}(f(\boldsymbol{x}') \neq y), \tag{2}$$

where $\mathbb{1}(\cdot)$ is the indicator function. Similar to Madry et al. (2018); Wang et al. (2020b), in practice, we leverage the commonly used cross entropy (CE) loss as the surrogate loss of $\mathbb{1}(f(\boldsymbol{x}') \neq y)$ and minimize it by projected gradient descent (PGD).

Note that Equation 2 looks similar to but conceptually differs from the known targeted adversarial attack (Carlini & Wagner, 2017), which generates a kind of adversarial examples defined on correctly classified clean inputs and targeted to wrong classes. The hypocritical examples here are defined on misclassified inputs and are targeted to their right classes.

2.1 ATTACK RESULTS

In this subsection, we demonstrate the power of our proposed hypocritical attack on three benchmark datasets: MNIST (LeCun et al., 1998), CIFAR-10 (Krizhevsky et al., 2009) and ImageNet (Russakovsky et al., 2015).

Table 1: Accuracy ($\%$) evaluated on MNIST. Attacks are bounded with $\epsilon = 0.2$.

Model	$\mathcal{F}$	$\mathcal{D}$	$\mathcal{A}$
Naive (MLP)	100.0	10.4	0.0
Naive (LeNet)	79.2	10.1	0.0
Standard (MLP)	100.0	97.8	29.8
Standard (LeNet)	100.0	99.4	0.1

Table 2: Accuracy ($\%$) evaluated on ImageNet. Attacks are bounded with $\epsilon = 16/255$.

Model	$\mathcal{F}$	$\mathcal{D}$	$\mathcal{A}$
Naive (VGG16)	100.0	0.1	0.0
Naive (ResNet50)	12.6	0.1	0.0
Standard (VGG16)	99.9	71.6	0.3
Standard (ResNet50)	99.9	76.1	0.0

We attack models trained with standard approach using clean examples (Standard) and models that randomly initialized without training (Naive). For MNIST, the hypocritically perturbed set $\mathcal{F}$ and the adversarially perturbed set $\mathcal{A}$ are constructed by attacking every example in the clean test set sampled from $\mathcal{D}$. Both attacks are bounded by a l_∞ ball with radius $\epsilon = 0.2$. For ImageNet, $\mathcal{F}$ and $\mathcal{A}$ are constructed based on its validation set sampled from $\mathcal{D}$. Both attacks are bounded by a l_∞ ball with radius $\epsilon = 16/255$. For each experiment, we conduct 3 trials with different random seeds and report the averaged result to reduce the impact of random variations. Appendix A.2 describes further experimental details about DNN architecture, training procedure and more results.

Results on MNIST and ImageNet are summarized in Table 1 and Table 2, respectively. First, we find that the naturally trained models are extremely sensitive to hypocritical perturbations (e.g., Standard (MLP) and Standard (LeNet) achieve 100% accuracy on hypocritically perturbed MNIST test set, and Standard (VGG16) and Standard (ResNet50) achieve 99% accuracy on hypocritically perturbed ImageNet validation set). Second, we find that part of randomly initialized models is extremely sensitive (e.g., Naive (MLP) and Naive (VGG16) achieve 100% accuracy on $\mathcal{F}$ of MNIST and ImageNet). These results demonstrate the unreliability of standard evaluation process in the existence of false friends. Once a "well-performed" model (such as Naive (MLP) or Naive (VGG16)) is permitted to be deployed in real-world applications due to that the deployer has a false sense of performance, potential security concerns appear even in benign environments.

It seems that the Naive (ResNet50) model is relatively robust to hypocritical examples on ImageNet. But that is just a trivial defense, it simply predicts most of the points in input region as a certain class because of the poor scaling of network weights at initialization (He et al., 2016b; Elsayed et al., 2019). More discussions are in Appendix A.2. Therefore, it is not enough to blindly pursue robustness against hypocritical perturbations but ignore the performance on clean examples.

3 HYPOCRITICAL RISK

In this section, we formalize the hypocritical risk and analyze the relation between natural risk, adversarial risk, and hypocritical risk. We propose a defense method specialized for hypocritical examples by minimizing the tradeoff between natural risk and an upper bound of the hypocritical risk. Moreover, by decomposing a existing method designed for adversarial defense (TRADES (Zhang et al., 2019)), we find that, surprisingly, TRADES minimizes not only the adversarial risk on correctly classified examples, but also a looser upper bound of the hypocritical risk. Our theoretical analysis suggests that TRADES can be another candidate defense method for hypocritical examples.

3.1 THEORETICAL ANALYSIS

To characterize the adversarial robustness of a classifier f, Madry et al. (2018); Uesato et al. (2018); Cullina et al. (2018) defined the *adversarial risk* under the threat model of bounded ϵ ball:

$$\mathcal{R}_{\mathsf{adv}}(f) = \mathop{\mathbb{E}}_{(\boldsymbol{x},y)\sim\mathcal{D}} \left[\max_{\boldsymbol{x}'\in\mathcal{B}_\epsilon(\boldsymbol{x})} \mathbb{1}(f(\boldsymbol{x}') \neq y) \right]. \tag{3}$$

The standard measure of classifier performance, known as *natural risk*, is denoted as $\mathcal{R}_{\mathsf{nat}}(f) = \mathbb{E}_{(\boldsymbol{x},y)\sim\mathcal{D}} [\mathbb{1}(f(\boldsymbol{x}) \neq y)]$. Let $q(\boldsymbol{x}, y)$ be the probability density function of data distribution $\mathcal{D}$. We denote by $\mathcal{S}_f^+$ the conditional data distribution on correctly classified examples w.r.t. f, with a conditional density function $q(\boldsymbol{x}, y \mid E) = q(\boldsymbol{x}, y)/\,\mathrm{Z}(E)$ if E is true (otherwise $q(\boldsymbol{x}, y \mid E) = 0$), where the event E is $f(\boldsymbol{x}) = y$ and $\mathrm{Z}(E) = \int_{\boldsymbol{x},y} \mathbb{1}(f(\boldsymbol{x}) = y) dq(\boldsymbol{x}, y)$ is a normalizing constant. We denote by $\mathcal{S}_f^-$ the conditional data distribution on misclassified examples with the conditional density function $q(\boldsymbol{x}, y \mid E)$ and $f(\boldsymbol{x}) \neq y$ as the event E. Then we have the following relation between the natural risk and the adversarial risk:

Proposition 1. *Denote the adversarial risk on correctly classified examples by*

$$\hat{\mathcal{R}}_{\mathsf{adv}}(f) = \mathop{\mathbb{E}}_{(\boldsymbol{x},y)\sim\mathcal{S}_f^+} \left[\max_{\boldsymbol{x}'\in\mathcal{B}_\epsilon(\boldsymbol{x})} \mathbb{1}(f(\boldsymbol{x}') \neq y) \right],$$

then we have

$$\mathcal{R}_{\mathsf{adv}}(f) = \mathcal{R}_{\mathsf{nat}}(f) + (1 - \mathcal{R}_{\mathsf{nat}}(f))\hat{\mathcal{R}}_{\mathsf{adv}}(f).$$

Proposition 1 shows that we can view the adversarial risk $\mathcal{R}_{\mathsf{adv}}(f)$ as the tradeoff between $\mathcal{R}_{\mathsf{nat}}(f)$ and $\hat{\mathcal{R}}_{\mathsf{adv}}(f)$ with the scaling parameter $\lambda = 1 - \mathcal{R}_{\mathsf{nat}}(f)$. The adversarial risk on correctly classified examples $\hat{\mathcal{R}}_{\mathsf{adv}}(f)$ is in sharp contrast to the hypocritical risk defined on misclassified examples formalized as follows:

Definition 3 (Hypocritical Risk)**.** *The hypocritical risk on misclassified examples of a classifier f under the threat model of bounded ϵ ball is defined as*

$$\hat{\mathcal{R}}_{\mathsf{hyp}}(f) = \mathop{\mathbb{E}}_{(\boldsymbol{x},y)\sim\mathcal{S}_f^-} \left[\max_{\boldsymbol{x}'\in\mathcal{B}_\epsilon(\boldsymbol{x})} \mathbb{1}(f(\boldsymbol{x}') = y) \right].$$

The hypocritical risk $\hat{\mathcal{R}}_{\mathsf{hyp}}(f)$ is the proportion of perturbed examples (originally misclassified) that can be successfully correctly classified by the classifier after a false friend's attack. However, it's hard to do optimization over $\hat{\mathcal{R}}_{\mathsf{hyp}}(f)$. To ease the optimization obstacles in there, we derive the following upper bounds.

Theorem 1. *For any data distribution $\mathcal{D}$ and its corresponding conditional distribution on misclassified examples $\mathcal{S}_f^-$ w.r.t. a classifier f, we have*

$$\underbrace{\mathop{\mathbb{E}}_{(\boldsymbol{x},y)\sim\mathcal{S}_f^-} \mathbb{1}(f(\boldsymbol{x}_{\mathsf{hyp}}) = y)}_{\hat{\mathcal{R}}_{\mathsf{hyp}}(f)} \leq \underbrace{\mathop{\mathbb{E}}_{(\boldsymbol{x},y)\sim\mathcal{S}_f^-} \mathbb{1}(f(\boldsymbol{x}_{\mathsf{hyp}}) \neq f(\boldsymbol{x}))}_{\overline{\mathcal{R}}_{\mathsf{hyp}}(f)} \leq \underbrace{\mathop{\mathbb{E}}_{(\boldsymbol{x},y)\sim\mathcal{S}_f^-} \mathbb{1}(f(\boldsymbol{x}_{\mathsf{rev}}) \neq f(\boldsymbol{x}))}_{\overline{\overline{\mathcal{R}}}_{\mathsf{hyp}}(f)},$$

where $\boldsymbol{x}_{\mathsf{hyp}} = \mathop{\arg\max}_{\boldsymbol{x}'\in\mathcal{B}_\epsilon(\boldsymbol{x})} \mathbb{1}(f(\boldsymbol{x}') = y)$ *and* $\boldsymbol{x}_{\mathsf{rev}} = \mathop{\arg\max}_{\boldsymbol{x}'\in\mathcal{B}_\epsilon(\boldsymbol{x})} \mathbb{1}(f(\boldsymbol{x}') \neq f(\boldsymbol{x}))$.

Here $\boldsymbol{x}_{\mathsf{rev}}$ means that it pursues to reverse a clean example to a different class, from the point of view of the model. The upper bounds found in Theorem 1 allow us to optimize the hypocritical risk using proper surrogate loss functions which are both physical meaningful and computaionally tractable. Before we move forward to algorithmic design, we state a useful proposition below, which reveals the internal mechanism behind in TRADES.

Proposition 2. $\mathcal{R}_{\mathsf{rev}}(f) = (1-\mathcal{R}_{\mathsf{nat}}(f))\hat{\mathcal{R}}_{\mathsf{adv}}(f)+\mathcal{R}_{\mathsf{nat}}(f)\overline{\overline{\mathcal{R}}}_{\mathsf{hyp}}(f) = \mathop{\mathbb{E}}_{(\boldsymbol{x},y)\sim\mathcal{D}} \mathbb{1}(f(\boldsymbol{x}_{\mathsf{rev}}) \neq f(\boldsymbol{x}))$.

Proposition 2 shows a connection between adversarial risk and hypocritical risk: the adversarial risk on correctly classified examples $\hat{\mathcal{R}}_{\mathsf{adv}}(f)$ and the looser upper bound of the hypocritical risk on misclassified examples $\overline{\overline{\mathcal{R}}}_{\mathsf{hyp}}(f)$ can be seamlessly united to a new risk on all examples $\mathcal{R}_{\mathsf{rev}}(f)$. We name it *reversible risk* since minimizing it pursues the model whose predictions can't be reversed by small perturbations.

3.2 Algorithmic design

Now we are ready to design objective functions that improve model robustness against hypocritical examples while keeping model accuracy on clean examples.

Similar to (Zhang et al., 2019; Wang et al., 2020b; Tramèr et al., 2020; Raghunathan et al., 2020), we propose a defense objective by minimizing the tradeoff between the natural risk and the tighter upper bound of the hypocritical risk:

$$\mathcal{R}_{\mathsf{THRM}}(f) = \mathcal{R}_{\mathsf{nat}}(f) + \lambda\overline{\mathcal{R}}_{\mathsf{hyp}}(f), \tag{4}$$

where $\lambda > 0$ is a tunable scaling parameter balancing the importance of natural risk and hypocritical risk. We name our method **THRM** (Tradeoff for Hypocritical Risk Minimization).

Optimization over 0-1 loss in THRM is still intractable. In practice, for the indicator function $\mathbb{1}(f(\boldsymbol{x}) \neq y)$ in $\mathcal{R}_{\mathsf{nat}}(f)$, we adopt the commonly used CE loss as surrogate loss. Observed that $\overline{\mathcal{R}}_{\mathsf{hyp}}(f) = \frac{1}{\mathcal{R}_{\mathsf{nat}}(f)}\mathbb{E}_{(\boldsymbol{x},y)\sim\mathcal{D}}\mathbb{1}(f(\boldsymbol{x}_{\mathsf{hyp}}) \neq f(\boldsymbol{x}))$, we absorb the $\mathcal{R}_{\mathsf{nat}}(f)$ term into λ and use KL divergence as the surrogate loss of the indicator function $\mathbb{1}(f(\boldsymbol{x}_{\mathsf{hyp}}) \neq f(\boldsymbol{x}))$ (Zheng et al., 2016; Zhang et al., 2019; Wang et al., 2020b), since $f(\boldsymbol{x}_{\mathsf{hyp}}) \neq f(\boldsymbol{x})$ implies that the perturbed examples have different output distributions to that of clean examples. Our final objective function for THRM becomes

$$\mathcal{L}_{\mathsf{THRM}} = \mathop{\mathbb{E}}_{(\boldsymbol{x},y)\sim\mathcal{D}} \left[\mathcal{L}_{\mathsf{CE}}(p(\boldsymbol{x}), y) + \lambda\mathcal{L}_{\mathsf{KL}}(p(\boldsymbol{x}), p(\boldsymbol{x}_{\mathsf{hyp}}))\right]. \tag{5}$$

Intuition behind the objective $\mathcal{L}_{\mathsf{THRM}}$: the first term in Equation 5 encourages the natural risk to be optimized, while the second regularization term encourages the output to be stable against hypocritical perturbations, that is, the classifier should not be overly confident in its predictions especially when a false friend wants it to be.

To derive the objective function for TRADES, we can minimize the tradeoff between the natural risk and the reversible risk:

$$\mathcal{R}_{\mathsf{TRADES}}(f) = \mathcal{R}_{\mathsf{nat}}(f) + \lambda\mathcal{R}_{\mathsf{rev}}(f). \tag{6}$$

Similar to THRM, we use CE loss and KL divergence as the surrogate loss of $\mathbb{1}(f(\boldsymbol{x}) \neq y)$ and $\mathbb{1}(f(\boldsymbol{x}_{\mathsf{rev}}) \neq f(\boldsymbol{x}))$, respectively. The final objective function becomes

$$\mathcal{L}_{\mathsf{TRADES}} = \mathop{\mathbb{E}}_{(\boldsymbol{x},y)\sim\mathcal{D}} \left[\mathcal{L}_{\mathsf{CE}}(p(\boldsymbol{x}), y) + \lambda\mathcal{L}_{\mathsf{KL}}(p(\boldsymbol{x}), p(\boldsymbol{x}_{\mathsf{rev}}))\right], \tag{7}$$

which is exactly the multi-class classification objective function first proposed in Zhang et al. (2019) for adversarial defense. From the perspective of the hypocritical risk, our Proposition 2 reveals an advantage behind it, that is, TRADES is capable of minimizing the upper bound of hypocritical risk $\overline{\overline{\mathcal{R}}}_{\mathsf{hyp}}(f)$, thus can be considered as a candidate defense method for hypocritical examples. Proposition 2 also implies that there may be a deeper connection between adversarial robustness and hypocritical robustness. We will discuss it more and compare our proposed THRM with TRADES in next section.

4 TRADEOFF BETWEEN NATURAL AND HYPOCRITICAL RISKS

In this section, we show that there exists an inherent tension between the goal of natural risk minimization and hypocritical risk minimization. Thus the objective of model selection becomes to find the model which has better tradeoff between natural and hypocritical risks.

4.1 A TOY EXAMPLE

To illustrate the phenomenon, we first provide a toy example here, which is modified from the example in Zhang et al. (2019), and its risk minimization solutions can be analytically found.

Consider the case $(x, y) \in \mathbb{R} \times \{-1, +1\}$ from a distribution $\mathcal{D}$, where the marginal distribution over the instance space is a uniform distribution over $[0, 1]$, and for $k = 0, 1, \cdots, \lceil \frac{1}{2\epsilon} - 1 \rceil$,

$$\begin{aligned} \eta(x) &:= \Pr(y = +1 \mid x) \\ &= \begin{cases} 1/4, & x \in [2k\epsilon, (2k+1)\epsilon), \\ 1, & x \in ((2k+1)\epsilon, (2k+2)\epsilon]. \end{cases} \end{aligned} \tag{8}$$

In this problem, the solution for the objective in Equation 4 tends to the Bayes optimal classifier when $\lambda \to 0$, and tends to the all-one classifier when $\lambda \to +\infty$. Table 3 displays the trade-off between natural and hypocritical risks: the minimal natural risk $1/8$ is achieved by the Bayes optimal classifier $\mathrm{sign}(2\eta(x) - 1)$ with large hypocritical hypocritical risk, while the optimal hypocritical risk 0 is achieved by the all-one classifier with large natural risk.

Table 3: Comparison of Bayes optimal classifier and all-one classifier.

	Bayes Optimal Classifier	All-One Classifier
$\mathcal{R}_{\mathsf{nat}}$	$1/8$ (optimal)	$3/8$
$\hat{\mathcal{R}}_{\mathsf{hyp}}$	1	0 (optimal)

4.2 BENCHMARK EXPERIMENTS

To further demonstrate the tradeoff between natural and hypocritical risks and the effectiveness of methods proposed in Section 3.2, we conduct experiments on real-world datasets including MNIST and CIFAR-10.

We evaluate models trained using the objectives of THRM and TRADES with a wide range of scaling parameter λ. On MNIST, perturbations are bounded by l_∞ norm with $\epsilon = 0.2$. On CIFAR-10, models are trained against 3 different false friends bounded by l_∞ norm with $\epsilon = 1/255$, $\epsilon = 2/255$ and $\epsilon = 8/255$, respectively. Note that the hypocritical risk reported here is actually an approximation of the real value, since the optimization problem in it is NP-hard and we approximately solve it using surrogate loss and PGD on test set. Further details about model architecture and training procedure are in Appendix A.3.

Results on MNIST ($\epsilon = 0.2$) and CIFAR10 ($\epsilon = 2/255$) are shown in Figure 2. Each data point represents a model trained with different λ. More results including comparison with Madry's defense (Madry et al., 2018) are provided in Appendix A.3 due to the limited space. First, we observe that, on both datasets, as the regularization parameter λ increases, the natural risk $\mathcal{R}_{\mathsf{nat}}$ increases while the hypocritical risk $\hat{\mathcal{R}}_{\mathsf{hyp}}$ decreases, which verifies the effectiveness of our proposed method and the theoretical analysis in Proposition 2, where we reveal that TRADES is capable of minimizing a looser upper bound of hypocritical risk. Second, we show that THRM achieves better tradeoff on MNIST since it optimizes a tighter upper bound than TRADES. However, the situation becomes nuanced on CIFAR-10. As we can see in Figure 2(b), THRM seems to behave better in the beginning when λ is small but is surpassed by TRADES when λ increases. Overall, optimizing only a tighter upper bound of hypocritical risk achieves better tradeoff on test set when the task is relatively simple (e.g., on MNIST with $\epsilon = 0.2$), while simultaneously optimizing hypocritical risk and adversarial risk achieves better tradeoff on test set when the task tends to be hard (e.g., on CIFAR-10

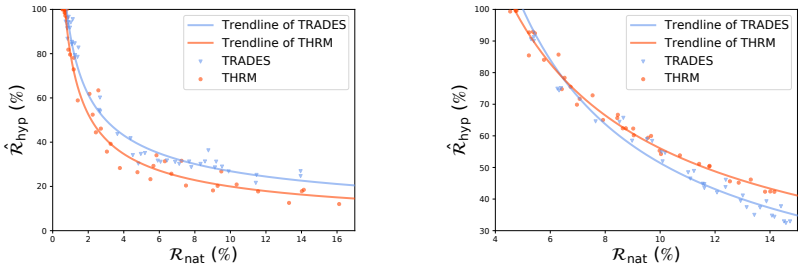

(a) On MNIST. Perturbations are bounded by l_∞ norm with $\epsilon = 0.2$.

(b) On CIFAR-10. Perturbations are bounded by l_∞ norm with $\epsilon = 2/255$.

Figure 2: Tradeoff between natural risk and hypocritical risk on real-world datasets.

with $\epsilon = 2/255$ and $\epsilon = 8/255$). This phenomenon shows that better adversarial robustness may help the generalization of hypocritical robustness, which conforms our intuition that they are two sides of the same coin. Thus there may be potential mutual benefits between them. After all, robust training objectives force DNNs to be invariant to signals that humans are invariant to, which may lead to feature representations that are more similar to what humans use (Salman et al., 2020). A rigorous treatment is beyond the scope of the current paper but is an important future direction.

5 Transferability Analysis

Transferability of adversarial examples across models is well known (Tramèr et al., 2017; Papernot et al., 2017b; Ilyas et al., 2019) and here we examine the transferability of hypocritical examples on MNIST and CIFAR-10. We observe that hypocritical examples, *i)* can transfer easily between naturally trained models, *ii)* are hard to transfer from randomly initialized models to other models (and vise versa), *iii)* are hard to transfer from standard models to defended models, *iv)* generated from THRM models usually have high transferability. Experimental details are in Appendix A.4. Better transferability is beneficial for black-box attacks but is not always desired by false friends. As a false friend, an attacker only expects high transferability on the targeted model the attacker chose to fool. If there are other competitive models available to the deployer, the attacker actually does not want the hypocritical examples to be successfully transferred to those competitive models. Thus fine-grained attack methods are required. We leave this to future work.

6 Discussion

The false friends considered in this paper are as powerful as typical adversaries. They all know the ground truth labels of clean examples. Such powerful friends actually can help a model to not only correctly classify a misclassified clean example but also correctly classify an adversarial example crafted by an adversary. One may expect to rely on true friends against adversaries. Unfortunately, an omniscient and faithful friend is unachievable in practical tasks, so far at least. Once it is achieved, the problem of robustness disappears immediately. What we can do at present is using a relatively more robust model as a surrogate of the true friend to improve the robustness of a weak model. This induces a promising general method in practice, that is, high-performance models can be employed as true friends to help a weak model without exposing training data and model weights for the purpose of privacy protection and knowledge transfer. Additional discussions are in Appendix C.

7 Conclusion

In this work, we expose a new risk arising from excessive sensitivity. Model performance becomes hypocritical in the existence of false friends. By formalizing the hypocritical risk and analyzing its relation with natural risk and adversarial risk, we propose to use THRM and TRADES as defense methods against hypocritical perturbations. Extensive experiments verify the effectiveness of methods. These findings open new avenues for mitigating and exploiting model sensitivity.

REFERENCES

Martin Abadi, Andy Chu, Ian Goodfellow, H Brendan McMahan, Ilya Mironov, Kunal Talwar, and Li Zhang. Deep learning with differential privacy. In *Proceedings of the 2016 ACM SIGSAC Conference on Computer and Communications Security*, pp. 308–318, 2016.

Anish Athalye, Nicholas Carlini, and David Wagner. Obfuscated gradients give a false sense of security: Circumventing defenses to adversarial examples. In *International Conference on Machine Learning (ICML)*, 2018.

Battista Biggio, Igino Corona, Davide Maiorca, B Nelson, N Srndic, P Laskov, Giorgio Giacinto, and Fabio Roli. Evasion attacks against machine learning at test time. In *Joint European conference on machine learning and knowledge discovery in databases (ECML PKDD)*, 2013.

Nicholas Carlini and David Wagner. Towards evaluating the robustness of neural networks. In *2017 IEEE symposium on security and privacy (sp)*, 2017.

Nicholas Carlini, Anish Athalye, Nicolas Papernot, Wieland Brendel, Jonas Rauber, Dimitris Tsipras, Ian Goodfellow, Aleksander Madry, and Alexey Kurakin. On evaluating adversarial robustness. *arXiv preprint arXiv:1902.06705*, 2019.

Lin Chen, Yifei Min, Mingrui Zhang, and Amin Karbasi. More data can expand the generalization gap between adversarially robust and standard models. In *International Conference on Machine Learning (ICML)*, 2020.

Daniel Cullina, Arjun Nitin Bhagoji, and Prateek Mittal. Pac-learning in the presence of adversaries. In *Advances in Neural Information Processing Systems (NeurIPS)*, 2018.

Edgar Dobriban, Hamed Hassani, David Hong, and Alexander Robey. Provable tradeoffs in adversarially robust classification. *arXiv preprint arXiv:2006.05161*, 2020.

Yinpeng Dong, Fangzhou Liao, Tianyu Pang, Hang Su, Jun Zhu, Xiaolin Hu, and Jianguo Li. Boosting adversarial attacks with momentum. In *Proceedings of the IEEE conference on computer vision and pattern recognition (CVPR)*, 2018.

Gamaleldin Elsayed, Shreya Shankar, Brian Cheung, Nicolas Papernot, Alexey Kurakin, Ian Goodfellow, and Jascha Sohl-Dickstein. Adversarial examples that fool both computer vision and time-limited humans. In *Advances in Neural Information Processing Systems (NeurIPS)*, 2018.

Gamaleldin F. Elsayed, Ian Goodfellow, and Jascha Sohl-Dickstein. Adversarial reprogramming of neural networks. In *International Conference on Learning Representations (ICLR)*, 2019.

Justin Gilmer, Luke Metz, Fartash Faghri, Samuel S Schoenholz, Maithra Raghu, Martin Wattenberg, and Ian Goodfellow. Adversarial spheres. *arXiv preprint arXiv:1801.02774*, 2018.

Ian Goodfellow and Nicolas Papernot. Is attacking machine learning easier than defending it. *Blog post on Feb*, 15:2017, 2017.

Ian J Goodfellow, Jonathon Shlens, and Christian Szegedy. Explaining and harnessing adversarial examples. In *International Conference on Learning Representations (ICLR)*, 2015.

Alex Graves, Abdel-rahman Mohamed, and Geoffrey Hinton. Speech recognition with deep recurrent neural networks. In *2013 IEEE International Conference on Acoustics, Speech and Signal Processing (ICASSP)*. IEEE, 2013.

Kaiming He, Xiangyu Zhang, Shaoqing Ren, and Jian Sun. Delving deep into rectifiers: Surpassing human-level performance on imagenet classification. In *Proceedings of the IEEE International Conference on Computer Vision (ICCV)*, 2015.

Kaiming He, Xiangyu Zhang, Shaoqing Ren, and Jian Sun. Deep residual learning for image recognition. In *Proceedings of the IEEE Conference on Computer Vision and Pattern Recognition (CVPR)*, 2016a.

Kun He, Yan Wang, and John Hopcroft. A powerful generative model using random weights for the deep image representation. In *Advances in Neural Information Processing Systems (NeurIPS)*, 2016b.

Andrew Ilyas, Shibani Santurkar, Dimitris Tsipras, Logan Engstrom, Brandon Tran, and Aleksander Madry. Adversarial examples are not bugs, they are features. In *Advances in Neural Information Processing Systems (NeurIPS)*, 2019.

Saumya Jetley, Nicholas Lord, and Philip Torr. With friends like these, who needs adversaries? In *Advances in Neural Information Processing Systems (NeurIPS)*, 2018.

Alex Krizhevsky, Geoffrey Hinton, et al. Learning multiple layers of features from tiny images. 2009.

Alex Krizhevsky, Ilya Sutskever, and Geoffrey E Hinton. Imagenet classification with deep convolutional neural networks. In *Advances in neural information processing systems (NeurIPS)*, 2012.

Alexey Kurakin, Ian Goodfellow, and Samy Bengio. Adversarial examples in the physical world. In *International Conference on Learning Representations (ICLR) Workshops*, 2016.

Yann LeCun, Léon Bottou, Yoshua Bengio, and Patrick Haffner. Gradient-based learning applied to document recognition. *Proceedings of the IEEE*, 86(11):2278–2324, 1998.

Yanpei Liu, Xinyun Chen, Chang Liu, and Dawn Song. Delving into transferable adversarial examples and black-box attacks. In *International Conference on Learning Representations (ICLR)*, 2017.

Aleksander Madry, Aleksandar Makelov, Ludwig Schmidt, Dimitris Tsipras, and Adrian Vladu. Towards deep learning models resistant to adversarial attacks. In *International Conference on Learning Representations (ICLR)*, 2018.

Volodymyr Mnih, Koray Kavukcuoglu, David Silver, Andrei A Rusu, Joel Veness, Marc G Bellemare, Alex Graves, Martin Riedmiller, Andreas K Fidjeland, Georg Ostrovski, et al. Human-level control through deep reinforcement learning. *nature*, 518(7540):529–533, 2015.

Nicolas Papernot, Patrick McDaniel, Somesh Jha, Matt Fredrikson, Z Berkay Celik, and Ananthram Swami. The limitations of deep learning in adversarial settings. In *2016 IEEE European symposium on security and privacy (EuroS&P)*, 2016.

Nicolas Papernot, Martín Abadi, Ulfar Erlingsson, Ian Goodfellow, and Kunal Talwar. Semi-supervised knowledge transfer for deep learning from private training data. In *International Conference on Learning Representations (ICLR)*, 2017a.

Nicolas Papernot, Patrick McDaniel, Ian Goodfellow, Somesh Jha, Z Berkay Celik, and Ananthram Swami. Practical black-box attacks against machine learning. In *Proceedings of the 2017 ACM on Asia conference on computer and communications security (ASIA CCS)*, 2017b.

Yao Qin, Nicholas Carlini, Garrison Cottrell, Ian Goodfellow, and Colin Raffel. Imperceptible, robust, and targeted adversarial examples for automatic speech recognition. In *International Conference on Machine Learning (ICML)*, 2019.

Aditi Raghunathan, Sang Michael Xie, Fanny Yang, John Duchi, and Percy Liang. Understanding and mitigating the tradeoff between robustness and accuracy. In *International Conference on Machine Learning (ICML)*, 2020.

Leslie Rice, Eric Wong, and J Zico Kolter. Overfitting in adversarially robust deep learning. In *International Conference on Machine Learning (ICML)*, 2020.

Olga Russakovsky, Jia Deng, Hao Su, Jonathan Krause, Sanjeev Satheesh, Sean Ma, Zhiheng Huang, Andrej Karpathy, Aditya Khosla, Michael Bernstein, et al. Imagenet large scale visual recognition challenge. *International Journal of Computer Vision (IJCV)*, 115(3):211–252, 2015.

Hadi Salman, Andrew Ilyas, Logan Engstrom, Ashish Kapoor, and Aleksander Madry. Do adversarially robust imagenet models transfer better? *arXiv preprint arXiv:2007.08489*, 2020.

Karen Simonyan and Andrew Zisserman. Very deep convolutional networks for large-scale image recognition. In *International Conference on Learning Representations (ICLR)*, 2014.

Christian Szegedy, Wojciech Zaremba, Ilya Sutskever, Joan Bruna, Dumitru Erhan, Ian Goodfellow, and Rob Fergus. Intriguing properties of neural networks. In *International Conference on Learning Representations (ICLR)*, 2014.

Florian Tramèr, Nicolas Papernot, Ian Goodfellow, Dan Boneh, and Patrick McDaniel. The space of transferable adversarial examples. *arXiv preprint arXiv:1704.03453*, 2017.

Florian Tramèr, Jens Behrmann, Nicholas Carlini, Nicolas Papernot, and Jörn-Henrik Jacobsen. Fundamental tradeoffs between invariance and sensitivity to adversarial perturbations. In *International Conference on Machine Learning (ICML)*, 2020.

Florian Tramer, Nicholas Carlini, Wieland Brendel, and Aleksander Madry. On adaptive attacks to adversarial example defenses. *arXiv preprint arXiv:2002.08347*, 2020.

Jonathan Uesato, Brendan O'Donoghue, Pushmeet Kohli, and Aaron Oord. Adversarial risk and the dangers of evaluating against weak attacks. In *International Conference on Machine Learning (ICML)*, 2018.

Beilun Wang, Ji Gao, and Yanjun Qi. A theoretical framework for robustness of (deep) classifiers against adversarial examples. In *International Conference on Learning Representations (ICLR) Workshops*, 2017.

Hongjun Wang, Guangrun Wang, Ya Li, Dongyu Zhang, and Liang Lin. Transferable, controllable, and inconspicuous adversarial attacks on person re-identification with deep mis-ranking. In *Proceedings of the IEEE/CVF Conference on Computer Vision and Pattern Recognition (CVPR)*, 2020a.

Yisen Wang, Difan Zou, Jinfeng Yi, James Bailey, Xingjun Ma, and Quanquan Gu. Improving adversarial robustness requires revisiting misclassified examples. In *International Conference on Learning Representations (ICLR)*, 2020b.

Tsui-Wei Weng, Huan Zhang, Pin-Yu Chen, Jinfeng Yi, Dong Su, Yupeng Gao, Cho-Jui Hsieh, and Luca Daniel. Evaluating the robustness of neural networks: An extreme value theory approach. In *International Conference on Learning Representations (ICLR)*, 2018.

Dongxian Wu, Yisen Wang, Shu-Tao Xia, James Bailey, and Xingjun Ma. Skip connections matter: On the transferability of adversarial examples generated with resnets. In *International Conference on Learning Representations (ICLR)*, 2020a.

Tong Wu, Liang Tong, and Yevgeniy Vorobeychik. Defending against physically realizable attacks on image classification. In *International Conference on Learning Representations (ICLR)*, 2020b.

Kaidi Xu, Gaoyuan Zhang, Sijia Liu, Quanfu Fan, Mengshu Sun, Hongge Chen, Pin-Yu Chen, Yanzhi Wang, and Xue Lin. Adversarial t-shirt! evading person detectors in a physical world. In *Proceedings of the European Conference on Computer Vision (ECCV)*, 2020.

Sergey Zagoruyko and Nikos Komodakis. Wide residual networks. *arXiv preprint arXiv:1605.07146*, 2016.

Haichao Zhang and Jianyu Wang. Towards adversarially robust object detection. In *Proceedings of the IEEE International Conference on Computer Vision (ICCV)*, 2019.

Hongyang Zhang, Yaodong Yu, Jiantao Jiao, Eric Xing, Laurent El Ghaoui, and Michael Jordan. Theoretically principled trade-off between robustness and accuracy. In *International Conference on Machine Learning (ICML)*, 2019.

Jingfeng Zhang, Xilie Xu, Bo Han, Gang Niu, Lizhen Cui, Masashi Sugiyama, and Mohan Kankanhalli. Attacks which do not kill training make adversarial learning stronger. In *International Conference on Machine Learning (ICML)*, 2020.

Stephan Zheng, Yang Song, Thomas Leung, and Ian Goodfellow. Improving the robustness of deep neural networks via stability training. In *Proceedings of the IEEE Conference on Computer Vision and Pattern Recognition (CVPR)*, 2016.

A EXPERIMENTAL DETAILS

A.1 DETAILS IN FIGURE 1

Attack procedure. In adversarial attack, we perturb clean inputs to maximize the surrogate loss using PGD. In hypocritical attack, we perturb clean inputs to minimize the surrogate loss using PGD. In both attacks, for the purpose of imperceptibility, we execute PGD attack 100 steps (step size is $\epsilon/50$) with early stopping on ImageNet and the budget ϵ here is $2/255$.

More examples. More adversarial examples and hypocritical examples generated on ImageNet using our methods are shown in Figure 4. More hypocritical examples generated on MNIST and CIFAR-10 are shown in Figure 3(a) and Figure 3(b). The victim models are LeNet (Standard) and Wide ResNet (Standard) for MNIST and CIFAR-10, respectively. They are trained with the same procedures described in Appendix A.2. In both attacks, for the purpose of imperceptibility, we execute 100 steps PGD attacks (step size is $\epsilon/50$) with early stopping on MNIST and CIFAR-10. The budget ϵ for MNIST here is 0.2. The budget for CIFAR-10 here is $8/255$.

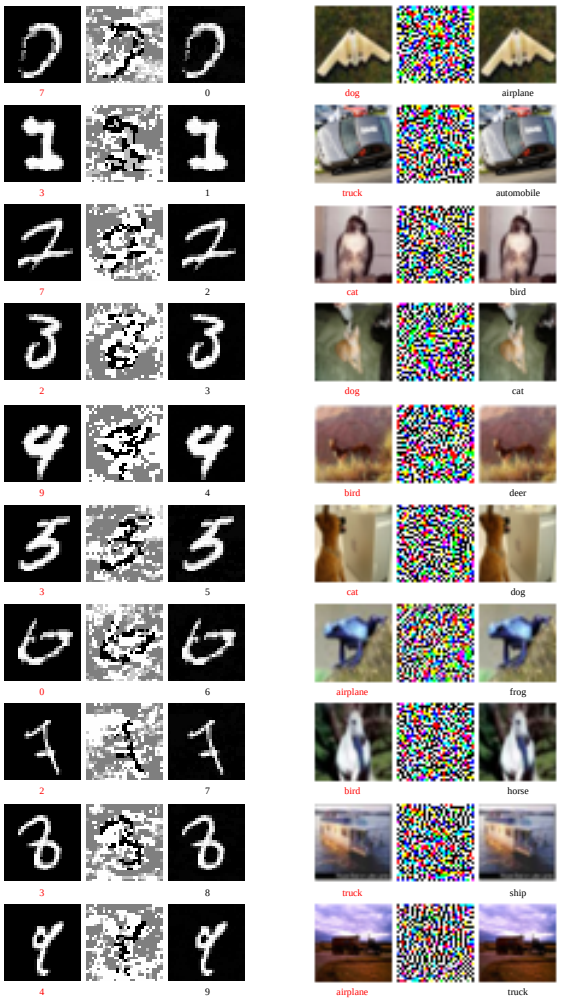

(a) On MNIST (b) On CIFAR-10

Figure 3: Hypocritical examples. In each subfigure, the first cloumn represents the clean examples sampled from original data distribution, the second cloumn represents the generated perturbations, the third cloumn represents the perturbed examples. Perturbations are rescaled for display. Red labels and black labels below images denote misclassification and correct classification, respectively.

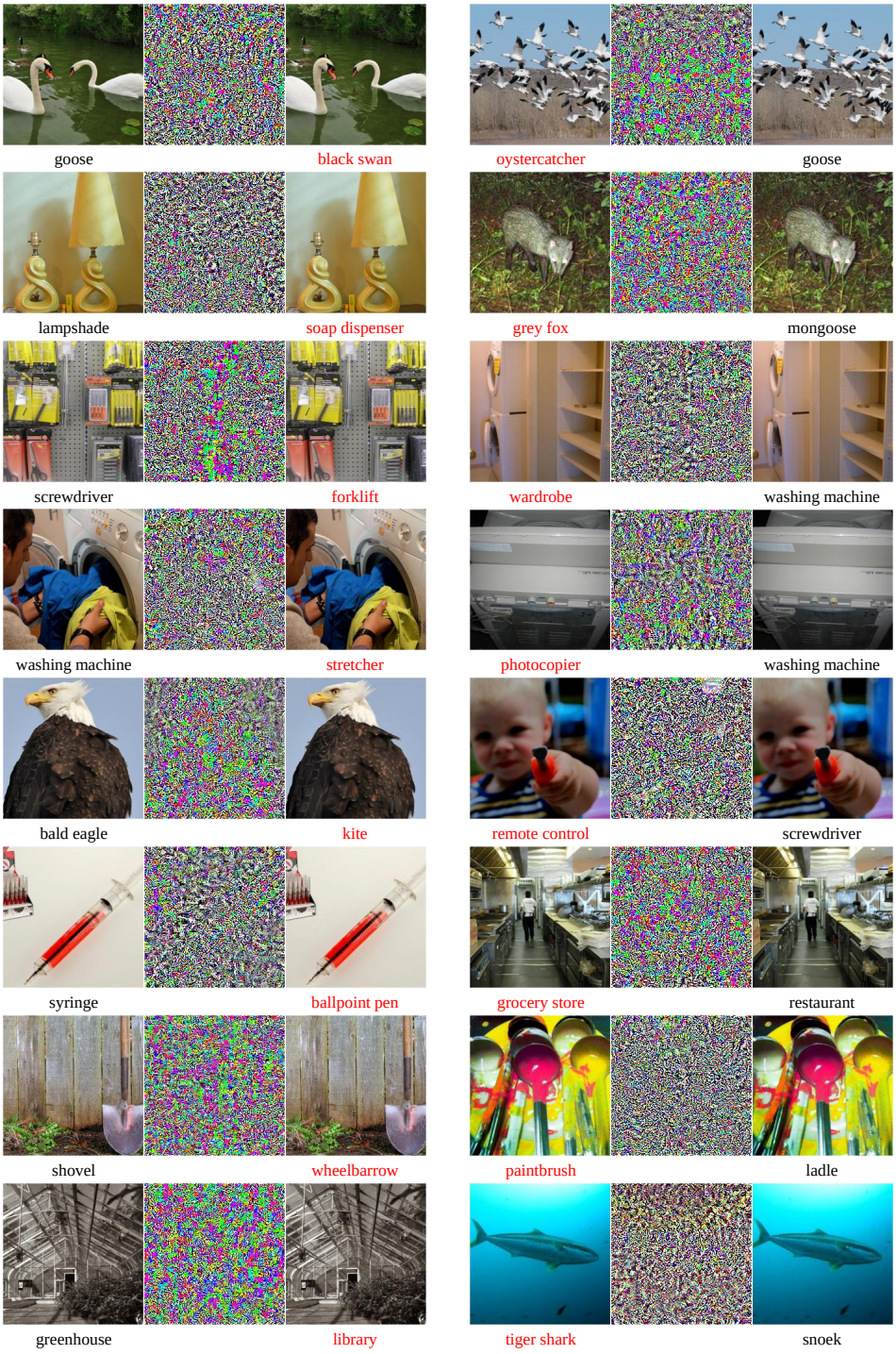

(a) Adversarial examples

(b) Hypocritical examples

Figure 4: More examples on ImageNet. In each subfigure, the first cloumn represents the clean examples sampled from original data distribution, the second cloumn represents the generated perturbations, the third cloumn represents the perturbed examples. Perturbations are rescaled for display. The model predictions of these images are shown below each image. Red labels and black labels below images denote misclassification and correct classification, respectively.

A.2 DETAILS IN SECTION 2.1

Architecture. For MNIST, a four-layer multilayer perception (MLP) (2 hidden layers, 768 neurons in each) with ReLU activations and a variant of LeNet model (2 convolutional layers of sizes 32 and 64, and a fully connected layer of size 1024) are adopted. For CIFAR-10, a four-layer MLP (2 hidden layers, 3072 neurons in each) with ReLU activations, a ResNet18 (He et al., 2016a) and a Wide ResNet (Zagoruyko & Komodakis, 2016) (with depth 28 and width factor 10) are adopted. For ImageNet, a VGG16 (Simonyan & Zisserman, 2014) and a ResNet50 (He et al., 2016a) are adopted.

Training procedure. *i)* Models trained with standard approach using clean examples (Standard). For MNIST, models are trained for 80 epochs with Adam optimizer with batch size 128 and a learning rate of 0.001. Early stopping is done with holding out 1000 examples from the MNIST training set. For CIFAR-10, models are trained for 150 epochs with SGD optimizer with batch size 128 and the learning rate starts with 0.1, and is divided it by 10 at 90 and 125 epochs. We apply weight decay of 2e-4 and momentum of 0.9. Early stopping is done with holding out 1000 examples from the CIFAR-10 training set. For ImageNet, we use the pretrained standard models available within PyTorch (torchvision.models). *ii)* Models that randomly initialized without training (Naive). For all models, we use the default PyTorch initialization, except that we initialize the convolutional weights in Wide ResNet with He initialization (He et al., 2015). We conduct all the experiments using a single NVIDIA Tesla V100 GPU. Each experiment is conducted 3 times with different random seeds, except the standard models trained on ImageNet, in which we use the pretrained standard models available within PyTorch.

Attack procedure. For adversarial attack, we perturb clean inputs to maximize the surrogate loss using PGD. For hypocritical attack, we perturb clean inputs to minimize the surrogate loss using PGD. For both attacks, we execute 50 steps PGD attacks (step size is $\epsilon/10$) with 20 times of random restart on MNIST and CIFAR-10, and we use 50 steps PGD attacks (step size is $\epsilon/8$) on ImageNet. Other hyperparameter choices didn't offer a significant change in accuracy. On MNIST, the hypocritical perturbed set $\mathcal{F}$ and the adversarially perturbed set $\mathcal{A}$ are constructed by attacking every example in the clean test set sampled from $\mathcal{D}$. Both attacks are bounded by a l_∞ ball with radius $\epsilon = 0.2$. On CIFAR-10, both attacks are bounded by a l_∞ ball with radius $\epsilon = 8/255$. On ImageNet, $\mathcal{F}$ and $\mathcal{A}$ are constructed based on its validation set sampled from $\mathcal{D}$. Both attacks are bounded by a l_∞ ball with radius $\epsilon = 16/255$.

Numerical results. The attack results on CIFAR-10 are shown in Table 4. Full results of Table 1, Table 2 and Table 4 are shown in Table 5, Table 6 and Table 7, respectively. Moreover, we show the attack results of 9 Naive models evaluated on ImageNet in Table 6. We find that all the Naive models in VGG family achieve high accuracy on $\mathcal{F}$ and all the Naive models in ResNet family have relatively poor performance on $\mathcal{F}$. Especially, the Naive (ResNet152) model in Trial 1 is invariant to hypocritical perturbations. Even in the existence of a strong false friend, the hypocritical performance is still as low as the clean performance (only 0.1%). We carefully examined the Naive (ResNet152) model and find that it's actually a trivial classifier, which purely classifies almost all the points in input region $[0, 1]^d$ as a certain class for some simple reasons, such as poor scaling of network weights at initialization. Therefore, it is not enough to blindly pursue robustness against hypocritical perturbations but ignore the performance on clean examples. Once we train a Naive model with clean examples, the model becomes vulnerable immediately (see Standard (ResNet50)), whereas the trained weights are better conditioned (Elsayed et al., 2019).

Table 4: Accuracy ($\%$) of models evaluated on CIFAR-10. Attacks are bounded with $\epsilon = 8/255$.

Model	$\mathcal{F}$	$\mathcal{D}$	$\mathcal{A}$
Naive (MLP)	92.3	9.9	0.0
Naive (ResNet18)	20.8	8.7	0.3
Naive (Wide ResNet)	13.8	10.0	6.9
Standard (MLP)	88.6	45.1	3.9
Standard (ResNet18)	100.0	94.1	0.0
Standard (Wide ResNet)	100.0	95.1	0.0

Table 5: Full results of accuracy (%) evaluated on MNIST. Attacks are bounded with $\epsilon = 0.2$.

Model	Trial 1			Trial 2			Trial 3		
	$\mathcal{F}$	$\mathcal{D}$	$\mathcal{A}$	$\mathcal{F}$	$\mathcal{D}$	$\mathcal{A}$	$\mathcal{F}$	$\mathcal{D}$	$\mathcal{A}$
Naive (MLP)	100.0	11.2	0.0	100.0	10.8	0.0	100.0	9.4	0.0
Naive (LeNet)	69.1	9.7	0.0	77.5	10.6	0.0	91.0	10.1	0.0
Standard (MLP)	100.0	98.0	31.1	100.0	97.7	30.4	100.0	97.7	28.1
Standard (LeNet)	100.0	99.4	0.1	100.0	99.4	0.1	100.0	99.3	0.0

Table 6: Full results of accuracy (%) evaluated on ImageNet. Attacks are bounded with $\epsilon = 16/255$.

Model	Trial 1			Trial 2			Trial 3		
	$\mathcal{F}$	$\mathcal{D}$	$\mathcal{A}$	$\mathcal{F}$	$\mathcal{D}$	$\mathcal{A}$	$\mathcal{F}$	$\mathcal{D}$	$\mathcal{A}$
Naive (VGG11)	100.0	0.1	0.0	100.0	0.1	0.0	100.0	0.1	0.0
Naive (VGG13)	100.0	0.1	0.0	100.0	0.1	0.0	100.0	0.1	0.0
Naive (VGG16)	100.0	0.1	0.0	100.0	0.1	0.0	100.0	0.1	0.0
Naive (VGG19)	100.0	0.1	0.0	100.0	0.1	0.0	100.0	0.1	0.0
Naive (ResNet18)	58.4	0.1	0.0	83.2	0.1	0.0	57.6	0.1	0.0
Naive (ResNet34)	7.4	0.1	0.0	12.5	0.1	0.0	10.4	0.1	0.0
Naive (ResNet50)	10.6	0.1	0.0	14.7	0.1	0.0	12.6	0.1	0.0
Naive (ResNet101)	0.3	0.1	0.1	0.2	0.1	0.1	0.3	0.1	0.1
Naive (ResNet152)	0.1	0.1	0.1	0.3	0.1	0.1	0.2	0.1	0.1
Standard (VGG16)	99.9	71.6	0.3	N/A	N/A	N/A	N/A	N/A	N/A
Standard (ResNet50)	99.9	76.1	0.0	N/A	N/A	N/A	N/A	N/A	N/A

A.3 Details in Section 4.2

Architecture. For MNIST, a variant of LeNet model (2 convolutional layers of sizes 32 and 64, and a fully connected layer of size 1024) is adopted. For CIFAR-10, a Wide ResNet (with depth 28 and width factor 10) is adopted.

Training procedure. For the wide range of scaling parameter λ, we conduct experiments in parallel over multiple NVIDIA Tesla V100 GPUs. Each experiment is conducted 3 times with different random seeds. For MNIST, all models (including Standard, Madry, TRADES, THRM) are trained for 80 epochs with Adam optimizer with batch size 128 and a learning rate of 0.001. Early stopping is done with holding out 1000 examples from the MNIST training set as suggested in Rice et al. (2020). For CIFAR-10, all models are trained for 150 epochs with SGD optimizer with batch size 128 and the learning rate starts with 0.1, and is divided it by 10 at 90 and 125 epochs. We apply weight decay of 2e-4 and momentum of 0.9. Early stopping is done with holding out 1000 examples from the CIFAR-10 training set as suggested in Rice et al. (2020).

Attack procedure. For the inner maximization in the objective function of THRM, we perturb clean inputs to minimize the CE loss as the surrogate loss. For the inner maximization in TRADES, we maximize the KL divergence as the surrogate loss. For the inner maximization in Madry, we maximize the CE loss as the surrogate loss. On MNIST, the training attack is PGD with random start and 10 iterations (step size $\epsilon/4$). On CIFAR-10, the training attack is PGD with random start and 10 iterations (step size $\epsilon/4$) when $\epsilon = 8/255$, and the training attack is PGD with random start and 7 iterations (step size $\epsilon/3$) when $\epsilon = 1/255$ and $\epsilon = 2/255$. On all experiments, the test attack is 50 steps PGD (step size is $\epsilon/10$) with 20 times of random restart. Other hyperparameter choices didn't offer a significant change in accuracy.

Numerical results. The natural risk reported here is estimated on test set. The hypocritical risk reported here is estimated on test set and is actually an approximation of the real value since we approximately solve the optimization problem by PGD on examples from test set. Results on MNIST ($\epsilon = 0.2$) and CIFAR-10 ($\epsilon = 1/255$, $\epsilon = 2/255$ and $\epsilon = 8/255$) are shown in Figure

Table 7: Full results of accuracy (%) evaluated on CIFAR-10. Attacks are bounded with $\epsilon = 8/255$.

Model	Trial 1			Trial 2			Trial 3		
	$\mathcal{F}$	$\mathcal{D}$	$\mathcal{A}$	$\mathcal{F}$	$\mathcal{D}$	$\mathcal{A}$	$\mathcal{F}$	$\mathcal{D}$	$\mathcal{A}$
Naive (MLP)	98.2	9.0	0.0	91.4	10.3	0.0	87.4	10.3	0.0
Naive (ResNet18)	14.8	10.0	0.6	20.7	9.2	0.2	27.0	6.9	0.0
Naive (Wide ResNet)	12.2	10.0	7.7	10.4	10.0	9.6	18.7	10.0	3.3
Standard (MLP)	89.1	46.2	3.6	88.4	44.8	3.8	88.3	44.5	4.2
Standard (ResNet18)	100.0	93.9	0.0	100.0	94.3	0.0	100.0	94.0	0.0
Standard (Wide ResNet)	100.0	95.0	0.0	100.0	95.1	0.0	100.0	95.3	0.0

5. Each point in Figure 5 represents one model trained with a certain λ. Full numerical results on MNIST ($\epsilon = 0.2$) and CIFAR-10 ($\epsilon = 1/255$, $\epsilon = 2/255$ and $\epsilon = 8/255$) can be found in Table 8, Table 9, Table 10 and Table 11, respectively. On MNIST ($\epsilon = 0.2$), THRM has better tradeoff than TRADES. However, when the task becomes hard, TRADES performs as well as or better than THRM. On CIFAR-10, as the task becomes harder (the larger the radius ϵ the harder the task), the gap between TRADES and THRM becomes larger. This phenomenon shows that better adversarial robustness may help the generalization of hypocritical robustness, especially when the task is hard. Moreover, we compare our methods with Madry et al. (2018)'s defense designed for adversarial robustness (denoted as Madry) [2] and standard training method (denoted as Standard). We summarize results in Table 12. For direct comparison, we pick a certain λ for each model trained by TRADES and THRM in each task. We observed that, in all tasks, Madry's defense has nonnegligible robustness on hypocritical examples, although there is no hypocritical risk or its upper bound in the objective function. This phenomenon indicates that optimizing only adversarial risk could bring a certain degree of robustness against hypocritical examples. While this experimental results partly support our hypothesis (i.e., the potential mutual benefits between robustness against adversarial perturbations and hypocritical perturbations), we do not take the evidence as an ultimate one and further exploration is needed. We note that the standard deviation becomes larger when λ is bigger in TRADES and THRM, which is attributed to optimization difficulty and result in more significant difference among different trials. Reducing the initial learning rate may mitigate this phenomenon.

Table 8: Full results of natural risk (%) and hypocritical risk (%) on MNIST. Attacks are bounded by l_∞ norm with $\epsilon = 0.2$.

(a) For TRADES.

λ	Trial 1		Trial 2		Trial 3	
	$\mathcal{R}_{\mathsf{nat}}$	$\hat{\mathcal{R}}_{\mathsf{hyp}}$	$\mathcal{R}_{\mathsf{nat}}$	$\hat{\mathcal{R}}_{\mathsf{hyp}}$	$\mathcal{R}_{\mathsf{nat}}$	$\hat{\mathcal{R}}_{\mathsf{hyp}}$
0.1	0.7	94.5	0.9	94.2	0.9	96.7
1	1.0	94.1	0.8	91.5	0.8	92.8
5	0.8	86.7	1.0	91.8	1.1	95.6
10	1.2	84.7	1.1	85.3	1.1	84.3
20	1.5	82.8	1.4	78.6	1.3	79.4
40	2.7	60.2	2.7	53.9	2.6	54.6
60	4.4	41.8	4.5	34.1	3.6	43.7
80	5.2	35.1	5.0	34.7	4.8	30.3
120	6.1	31.1	6.9	31.1	5.9	31.6
160	7.8	28.7	8.6	31.3	6.4	31.7
200	9.2	31.2	7.7	31.3	7.1	30.2
240	9.9	26.8	8.8	36.3	9.1	28.6
300	8.3	30.2	14.0	26.9	9.5	29.0
500	11.4	21.6	14.0	24.7	11.5	25.2

(b) For THRM.

λ	Trial 1		Trial 2		Trial 3	
	$\mathcal{R}_{\mathsf{nat}}$	$\hat{\mathcal{R}}_{\mathsf{hyp}}$	$\mathcal{R}_{\mathsf{nat}}$	$\hat{\mathcal{R}}_{\mathsf{hyp}}$	$\mathcal{R}_{\mathsf{nat}}$	$\hat{\mathcal{R}}_{\mathsf{hyp}}$
1	0.5	100.0	0.6	100.0	0.7	100.0
10	0.7	100.0	0.8	100.0	0.7	100.0
100	0.7	100.0	0.7	98.6	0.7	100.0
200	0.8	96.3	0.7	97.2	0.7	98.5
400	1.0	79.6	1.2	72.9	0.9	81.8
600	2.1	61.8	1.4	58.9	1.2	78.2
800	2.7	46.1	2.6	63.4	2.4	44.4
1000	3.3	39.3	3.1	35.7	2.3	52.4
2000	5.8	34.1	4.8	26.4	3.8	28.3
3000	7.3	31.6	14.0	17.8	7.5	20.4
4000	6.7	25.7	5.5	23.3	9.0	18.2
5000	10.4	20.9	5.7	29.3	11.6	17.7
6000	14.1	18.5	16.1	12.0	9.5	26.8
7000	13.3	12.6	6.3	31.4	9.3	20.3

[2] They actually optimize the adversarial risk in Equation 3 via surrogate loss.

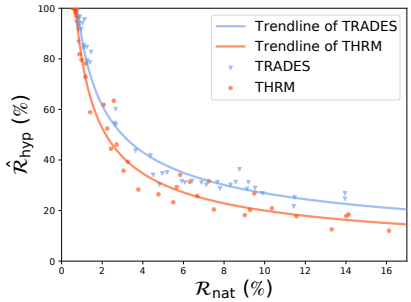

(a) On MNIST. Perturbations are bounded by l_∞ norm with $\epsilon = 0.2$.

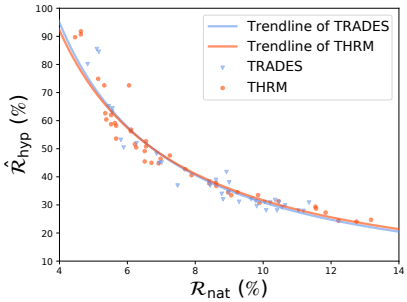

(b) On CIFAR-10. Perturbations are bounded by l_∞ norm with $\epsilon = 1/255$.

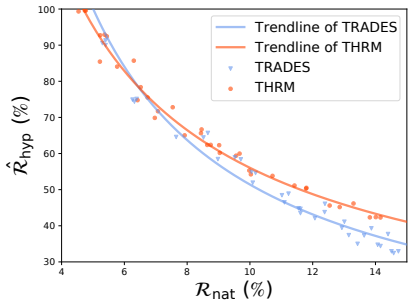

(c) On CIFAR-10. Perturbations are bounded by l_∞ norm with $\epsilon = 2/255$.

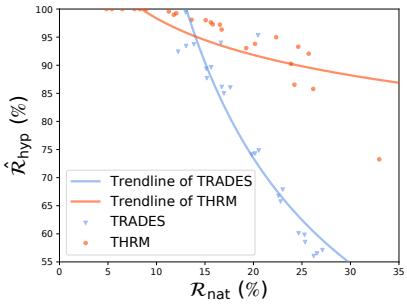

(d) On CIFAR-10. Perturbations are bounded by l_∞ norm with $\epsilon = 8/255$.

Figure 5: Tradeoff between natural risk and hypocritical risk on real-world datasets.

Table 9: Full results of natural risk (%) and hypocritical risk (%) on CIFAR-10. Attacks are bounded by l_∞ norm with $\epsilon = 1/255$.

(a) For TRADES.

λ	Trial 1		Trial 2		Trial 3	
	$\mathcal{R}_{\text{nat}}$	$\hat{\mathcal{R}}_{\text{hyp}}$	$\mathcal{R}_{\text{nat}}$	$\hat{\mathcal{R}}_{\text{hyp}}$	$\mathcal{R}_{\text{nat}}$	$\hat{\mathcal{R}}_{\text{hyp}}$
0.1	5.2	84.5	5.1	85.5	4.8	80.1
1	5.6	63.1	5.5	65.1	5.6	64.4
5	6.3	52.0	5.9	50.4	5.8	53.2
10	6.9	48.3	6.9	45.0	7.0	45.1
30	9.0	38.0	8.9	41.7	7.5	36.9
50	8.6	38.9	8.4	36.8	8.4	38.4
70	9.0	34.5	8.8	33.9	8.8	32.0
90	9.7	32.0	10.4	28.0	9.3	31.1
120	9.8	31.3	9.8	29.6	10.7	29.9
150	10.2	30.9	10.1	28.0	10.1	31.0
180	10.6	29.2	10.4	31.8	10.5	31.0
210	11.2	27.9	11.4	30.8	11.0	28.0

(b) For THRM.

λ	Trial 1		Trial 2		Trial 3	
	$\mathcal{R}_{\text{nat}}$	$\hat{\mathcal{R}}_{\text{hyp}}$	$\mathcal{R}_{\text{nat}}$	$\hat{\mathcal{R}}_{\text{hyp}}$	$\mathcal{R}_{\text{nat}}$	$\hat{\mathcal{R}}_{\text{hyp}}$
1	4.6	91.8	4.6	90.7	4.5	89.7
10	5.1	74.9	6.1	72.6	5.3	72.6
50	5.3	62.6	5.5	62.0	5.4	60.4
100	5.6	59.1	5.7	58.2	5.5	58.7
200	6.6	52.7	6.5	49.2	6.2	51.6
300	6.9	44.8	6.5	45.5	7.0	46.4
400	7.3	47.6	7.7	42.7	7.9	40.6
600	8.4	37.7	8.6	36.8	8.6	37.9
800	9.1	33.4	9.2	34.5	9.0	34.4
1000	9.9	30.7	9.8	33.5	10.5	31.4
1500	11.6	28.7	11.5	29.4	11.8	27.3
2000	13.2	24.7	12.2	24.4	12.8	24.1

Table 10: Full results of natural risk (%) and hypocritical risk (%) on CIFAR-10. Attacks are bounded by l_∞ norm with $\epsilon = 2/255$.

(a) For TRADES.

λ	Trial 1		Trial 2		Trial 3	
	$\mathcal{R}_{\mathsf{nat}}$	$\hat{\mathcal{R}}_{\mathsf{hyp}}$	$\mathcal{R}_{\mathsf{nat}}$	$\hat{\mathcal{R}}_{\mathsf{hyp}}$	$\mathcal{R}_{\mathsf{nat}}$	$\hat{\mathcal{R}}_{\mathsf{hyp}}$
0.1	5.4	91.3	5.3	90.6	5.4	90.0
1	6.3	74.4	6.3	74.9	6.4	75.1
5	8.5	64.4	7.7	64.6	8.7	65.7
10	9.7	58.4	9.0	58.5	9.5	58.9
30	10.2	54.6	10.1	51.9	10.1	54.9
50	11.1	46.5	11.2	48.9	11.0	48.5
70	11.6	44.7	11.6	43.5	11.6	44.8
90	12.1	42.1	12.4	46.1	12.4	43.8
120	13.2	37.4	13.0	41.1	12.9	39.4
150	13.6	37.3	13.9	39.3	13.4	35.0
180	14.1	34.8	14.2	34.4	14.4	37.7
210	14.7	32.9	14.6	32.4	14.5	32.9

(b) For THRM.

λ	Trial 1		Trial 2		Trial 3	
	$\mathcal{R}_{\mathsf{nat}}$	$\hat{\mathcal{R}}_{\mathsf{hyp}}$	$\mathcal{R}_{\mathsf{nat}}$	$\hat{\mathcal{R}}_{\mathsf{hyp}}$	$\mathcal{R}_{\mathsf{nat}}$	$\hat{\mathcal{R}}_{\mathsf{hyp}}$
1	4.8	99.6	4.5	99.3	4.7	99.6
10	5.4	92.9	5.4	92.5	5.2	92.7
50	6.3	85.7	5.8	84.1	5.2	85.4
100	6.7	75.5	6.4	74.8	6.5	78.4
150	7.1	71.7	7.0	69.9	7.5	72.8
200	8.4	65.6	7.9	65.0	8.5	66.7
250	8.8	62.4	8.6	62.4	9.0	62.3
300	9.6	59.4	9.0	60.2	9.7	60.0
400	10.0	54.2	10.0	55.3	10.7	53.8
600	11.8	50.5	11.4	51.1	11.8	50.3
800	12.5	45.6	12.9	45.2	13.3	46.2
1000	14.2	42.3	13.8	42.3	14.0	42.4

Table 11: Full results of natural risk (%) and hypocritical risk (%) on CIFAR-10. Attacks are bounded by l_∞ norm with $\epsilon = 8/255$.

(a) For TRADES.

λ	Trial 1		Trial 2		Trial 3	
	$\mathcal{R}_{\mathsf{nat}}$	$\hat{\mathcal{R}}_{\mathsf{hyp}}$	$\mathcal{R}_{\mathsf{nat}}$	$\hat{\mathcal{R}}_{\mathsf{hyp}}$	$\mathcal{R}_{\mathsf{nat}}$	$\hat{\mathcal{R}}_{\mathsf{hyp}}$
0.1	16.6	94.0	20.5	95.3	13.0	99.4
1	13.9	93.7	13.1	93.4	12.2	92.4
5	15.1	89.4	15.2	87.7	15.6	89.6
10	17.0	85.0	17.6	86.0	16.7	86.1
30	19.8	74.1	20.2	74.3	20.5	74.8
50	23.0	67.9	22.8	65.7	22.6	66.7
70	25.3	59.8	24.7	60.1	25.3	58.5
90	26.6	56.5	27.1	57.1	26.2	56.0

(b) For THRM.

λ	Trial 1		Trial 2		Trial 3	
	$\mathcal{R}_{\mathsf{nat}}$	$\hat{\mathcal{R}}_{\mathsf{hyp}}$	$\mathcal{R}_{\mathsf{nat}}$	$\hat{\mathcal{R}}_{\mathsf{hyp}}$	$\mathcal{R}_{\mathsf{nat}}$	$\hat{\mathcal{R}}_{\mathsf{hyp}}$
1	4.8	100.0	9.0	100.0	5.4	100.0
10	8.3	100.0	6.5	100.0	7.7	100.0
50	12.0	99.3	11.3	99.6	11.8	99.0
100	15.1	98.0	13.6	98.1	15.6	97.6
150	16.7	96.4	15.8	97.3	16.5	97.2
200	19.3	93.0	20.2	93.8	22.3	95.0
250	24.2	86.5	23.9	90.2	24.6	93.3
300	25.7	92.1	33.0	73.2	26.2	85.8

Table 12: Comparison of natural risk (%±std over 3 random trials) and hypocritical risk (%±std over 3 random trials) between methods on real-world datasets. Attacks are bounded by l_∞ norm.

(a) On MNIST ($\epsilon = 0.2$).

Method	$\mathcal{R}_{\mathsf{nat}}$	$\hat{\mathcal{R}}_{\mathsf{hyp}}$
Standard	0.6 ± 0.1	100.0 ± 0.0
Madry	0.9 ± 0.0	93.8 ± 1.5
TRADES ($\lambda = 240$)	9.3 ± 0.6	30.6 ± 5.1
THRM ($\lambda = 5000$)	9.2 ± 3.1	22.6 ± 6.0

(b) On CIFAR-10 ($\epsilon = 1/255$).

Method	$\mathcal{R}_{\mathsf{nat}}$	$\hat{\mathcal{R}}_{\mathsf{hyp}}$
Standard	4.9 ± 0.2	99.3 ± 0.3
Madry	5.3 ± 0.1	62.6 ± 0.1
TRADES ($\lambda = 150$)	10.1 ± 0.1	30.0 ± 1.7
THRM ($\lambda = 1000$)	10.1 ± 0.3	31.9 ± 1.4

(c) On CIFAR-10 ($\epsilon = 2/255$).

Method	$\mathcal{R}_{\mathsf{nat}}$	$\hat{\mathcal{R}}_{\mathsf{hyp}}$
Standard	4.8 ± 0.2	100 ± 0.0
Madry	6.3 ± 0.2	74.3 ± 1.0
TRADES ($\lambda = 150$)	13.6 ± 0.2	37.2 ± 2.2
THRM ($\lambda = 1000$)	14.0 ± 0.2	42.3 ± 0.0

(d) On CIFAR-10 ($\epsilon = 8/255$).

Method	$\mathcal{R}_{\mathsf{nat}}$	$\hat{\mathcal{R}}_{\mathsf{hyp}}$
Standard	4.7 ± 0.3	100.0 ± 0.0
Madry	14.2 ± 0.1	93.1 ± 1.0
TRADES ($\lambda = 50$)	22.8 ± 0.2	66.8 ± 1.1
THRM ($\lambda = 250$)	24.2 ± 0.4	90.0 ± 3.4

A.4 DETAILS IN SECTION 5

Hypocritical attack here is executed by 50 steps PGD (step size is $\epsilon/10$) on source models. Note that the optimization method we used here is not to pursue state-of-the-art transferability, but to examine the transferability of hypocritical examples. There are many methods designed to improve the transferability of adversarial examples may be extended to hypocritical examples (Liu et al., 2017; Dong et al., 2018; Wu et al., 2020a). Figure 6 shows the transferability heatmap of hypocritical attack over 9 models trained on MNIST. Figure 7 shows the transferability heatmap of hypocritical attack over 7 models trained on CIFAR-10. The value in the i-th row and j-th cloumn of each heatmap matrix is the proportion of the hypocritical examples successfully transferred to target model j out of all hypocritical examples generated by source model i (including both successful and failed attacks on the source model).

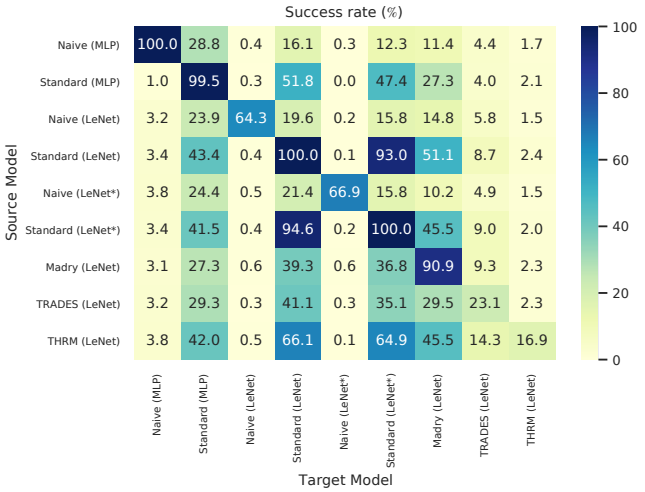

Figure 6: Transferability of hypocritical examples on MNIST. Attacks are bounded by l_∞ norm with $\epsilon = 0.2$. "(LeNet*)" means that it is the same architecture with "(LeNet)" but different random initialization.

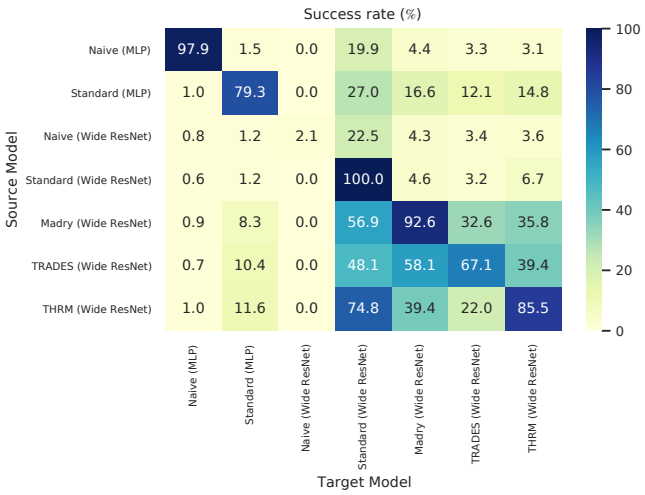

Figure 7: Transferability of hypocritical examples on CIFAR-10. Attacks are bounded by l_∞ norm with $\epsilon = 8/255$.

B PROOFS OF MAIN RESULTS

In this section, we provide the proofs of our main results.

B.1 A PROOF OF PROPOSITION 1

Proposition 1. *Denote the adversarial risk on correctly classified examples by*

$$\hat{\mathcal{R}}_{\mathsf{adv}}(f) = \mathop{\mathbb{E}}_{(\boldsymbol{x},y)\sim\mathcal{S}_f^+}\left[\max_{\boldsymbol{x}'\in\mathcal{B}_\epsilon(\boldsymbol{x})} \mathbb{1}(f(\boldsymbol{x}')\neq y)\right],$$

then we have

$$\mathcal{R}_{\mathsf{adv}}(f) = \mathcal{R}_{\mathsf{nat}}(f) + (1-\mathcal{R}_{\mathsf{nat}}(f))\hat{\mathcal{R}}_{\mathsf{adv}}(f).$$

Proof.

$$\begin{aligned}
\mathcal{R}_{\mathsf{adv}}(f) =& \mathop{\mathbb{E}}_{(\boldsymbol{x},y)\sim\mathcal{D}}\left[\max_{\boldsymbol{x}'\in\mathcal{B}_\epsilon(\boldsymbol{x})} \mathbb{1}(f(\boldsymbol{x}')\neq y)\right] \\
=& \mathop{\mathbb{E}}_{(\boldsymbol{x},y)\sim\mathcal{D}}\left[\mathbb{1}(f(\boldsymbol{x})=y)\cdot\max_{\boldsymbol{x}'\in\mathcal{B}_\epsilon(\boldsymbol{x})} \mathbb{1}(f(\boldsymbol{x}')\neq y)\right] \\
&+ \mathop{\mathbb{E}}_{(\boldsymbol{x},y)\sim\mathcal{D}}\left[\mathbb{1}(f(\boldsymbol{x})\neq y)\cdot\max_{\boldsymbol{x}'\in\mathcal{B}_\epsilon(\boldsymbol{x})} \mathbb{1}(f(\boldsymbol{x}')\neq y)\right] \\
=& \mathcal{R}_{\mathsf{nat}}(f)\mathop{\mathbb{E}}_{(\boldsymbol{x},y)\sim\mathcal{S}_f^-}\left[\max_{\boldsymbol{x}'\in\mathcal{B}_\epsilon(\boldsymbol{x})} \mathbb{1}(f(\boldsymbol{x}')\neq y)\right] \\
&+ (1-\mathcal{R}_{\mathsf{nat}}(f))\mathop{\mathbb{E}}_{(\boldsymbol{x},y)\sim\mathcal{S}_f^+}\left[\max_{\boldsymbol{x}'\in\mathcal{B}_\epsilon(\boldsymbol{x})} \mathbb{1}(f(\boldsymbol{x}')\neq y)\right] \\
=& \mathcal{R}_{\mathsf{nat}}(f)\mathop{\mathbb{E}}_{(\boldsymbol{x},y)\sim\mathcal{S}_f^-}[\mathbb{1}(f(\boldsymbol{x})\neq y)] + (1-\mathcal{R}_{\mathsf{nat}}(f))\mathop{\mathbb{E}}_{(\boldsymbol{x},y)\sim\mathcal{S}_f^+}\left[\max_{\boldsymbol{x}'\in\mathcal{B}_\epsilon(\boldsymbol{x})} \mathbb{1}(f(\boldsymbol{x}')\neq y)\right] \\
=& \mathcal{R}_{\mathsf{nat}}(f) + (1-\mathcal{R}_{\mathsf{nat}}(f))\mathop{\mathbb{E}}_{(\boldsymbol{x},y)\sim\mathcal{S}_f^+}\left[\max_{\boldsymbol{x}'\in\mathcal{B}_\epsilon(\boldsymbol{x})} \mathbb{1}(f(\boldsymbol{x}')\neq y)\right] \\
=& \mathcal{R}_{\mathsf{nat}}(f) + (1-\mathcal{R}_{\mathsf{nat}}(f))\hat{\mathcal{R}}_{\mathsf{adv}}(f).
\end{aligned}$$

□

B.2 A PROOF OF PROPOSITION 1

Theorem 1. *For any data distribution $\mathcal{D}$ and its corresponding conditional distribution on misclassified examples $\mathcal{S}_f^-$ w.r.t. a classifier f, we have*

$$\underbrace{\mathop{\mathbb{E}}_{(\boldsymbol{x},y)\sim\mathcal{S}_f^-}\mathbb{1}(f(\boldsymbol{x}_{\mathsf{hyp}})=y)}_{\hat{\mathcal{R}}_{\mathsf{hyp}}(f)} \leq \underbrace{\mathop{\mathbb{E}}_{(\boldsymbol{x},y)\sim\mathcal{S}_f^-}\mathbb{1}(f(\boldsymbol{x}_{\mathsf{hyp}})\neq f(\boldsymbol{x}))}_{\overline{\mathcal{R}}_{\mathsf{hyp}}(f)} \leq \underbrace{\mathop{\mathbb{E}}_{(\boldsymbol{x},y)\sim\mathcal{S}_f^-}\mathbb{1}(f(\boldsymbol{x}_{\mathsf{rev}})\neq f(\boldsymbol{x}))}_{\overline{\overline{\mathcal{R}}}_{\mathsf{hyp}}(f)},$$

where $\boldsymbol{x}_{\mathsf{hyp}} = \mathop{\arg\max}_{\boldsymbol{x}'\in\mathcal{B}_\epsilon(\boldsymbol{x})} \mathbb{1}(f(\boldsymbol{x}')=y)$ *and* $\boldsymbol{x}_{\mathsf{rev}} = \mathop{\arg\max}_{\boldsymbol{x}'\in\mathcal{B}_\epsilon(\boldsymbol{x})} \mathbb{1}(f(\boldsymbol{x}')\neq f(\boldsymbol{x}))$.

Proof. To prove the first inequality, we have

$$\begin{aligned}
\hat{\mathcal{R}}_{\mathsf{hyp}}(f) =& \mathop{\mathbb{E}}_{(\boldsymbol{x},y)\sim\mathcal{S}_f^-}\left[\max_{\boldsymbol{x}'\in\mathcal{B}_\epsilon(\boldsymbol{x})} \mathbb{1}(f(\boldsymbol{x}')=y)\right] \\
=& \mathop{\mathbb{E}}_{(\boldsymbol{x},y)\sim\mathcal{S}_f^-}\mathbb{1}(f(\boldsymbol{x}_{\mathsf{hyp}})=y) \\
\leq& \mathop{\mathbb{E}}_{(\boldsymbol{x},y)\sim\mathcal{S}_f^-}\mathbb{1}(f(\boldsymbol{x}_{\mathsf{hyp}})\neq f(\boldsymbol{x})),
\end{aligned}$$

where the above inequality involves two conditions:

$$\mathbb{1}(f(\boldsymbol{x}_{\mathsf{hyp}})=y)=\begin{cases} 1=\mathbb{1}(f(\boldsymbol{x}_{\mathsf{hyp}})\neq f(\boldsymbol{x})), & \text{if } f(\boldsymbol{x}_{\mathsf{hyp}})=y,\\ 0\leq\mathbb{1}(f(\boldsymbol{x}_{\mathsf{hyp}})\neq f(\boldsymbol{x})), & \text{if } f(\boldsymbol{x}_{\mathsf{hyp}})\neq y.\end{cases}$$

To prove the second inequality, we have

$$\begin{aligned}\overline{\mathcal{R}}_{\mathsf{hyp}}(f)&=\mathop{\mathbb{E}}_{(\boldsymbol{x},y)\sim\mathcal{S}_f^-}\mathbb{1}(f(\boldsymbol{x}_{\mathsf{hyp}})\neq f(\boldsymbol{x}))\\ &\leq\mathop{\mathbb{E}}_{(\boldsymbol{x},y)\sim\mathcal{S}_f^-}\mathbb{1}(f(\boldsymbol{x}_{\mathsf{rev}})\neq f(\boldsymbol{x}))\end{aligned}$$

Since $(\boldsymbol{x},y)\sim\mathcal{S}_f^-$, we have $f(\boldsymbol{x})\neq y$. If there exists a $\boldsymbol{x}_{\mathsf{hyp}}$ such that $f(\boldsymbol{x}_{\mathsf{hyp}})=y$, then $f(\boldsymbol{x}_{\mathsf{hyp}})\neq f(\boldsymbol{x})$. Now let $\boldsymbol{x}_{\mathsf{rev}}=\boldsymbol{x}_{\mathsf{hyp}}$, then $f(\boldsymbol{x}_{\mathsf{rev}})\neq f(\boldsymbol{x})$ is true. Otherwise, if we couldn't find a $\boldsymbol{x}_{\mathsf{hyp}}$ such that $f(\boldsymbol{x}_{\mathsf{hyp}})=y$, there still exists a posibility to find a $\boldsymbol{x}_{\mathsf{rev}}$ such that $f(\boldsymbol{x}_{\mathsf{rev}})\neq y$ but $f(\boldsymbol{x}_{\mathsf{rev}})\neq f(\boldsymbol{x})$ is true. Therefore, the above inequalities holds. □

B.3 A Proof of Proposition 2

Proposition 2. $\mathcal{R}_{\mathsf{rev}}(f)=(1-\mathcal{R}_{\mathsf{nat}}(f))\hat{\mathcal{R}}_{\mathsf{adv}}(f)+\mathcal{R}_{\mathsf{nat}}(f)\overline{\overline{\mathcal{R}}}_{\mathsf{hyp}}(f)=\mathop{\mathbb{E}}_{(\boldsymbol{x},y)\sim\mathcal{D}}\mathbb{1}(f(\boldsymbol{x}_{\mathsf{rev}})\neq f(\boldsymbol{x}))$.

Proof.

$$\begin{aligned}\mathcal{R}_{\mathsf{rev}}(f)=&(1-\mathcal{R}_{\mathsf{nat}}(f))\hat{\mathcal{R}}_{\mathsf{adv}}(f)+\mathcal{R}_{\mathsf{nat}}(f)\overline{\overline{\mathcal{R}}}_{\mathsf{hyp}}(f)\\ =&(1-\mathcal{R}_{\mathsf{nat}}(f))\mathop{\mathbb{E}}_{(\boldsymbol{x},y)\sim\mathcal{S}_f^+}[\mathbb{1}(f(\boldsymbol{x}_{\mathsf{adv}})\neq y)]+\mathcal{R}_{\mathsf{nat}}(f)\mathop{\mathbb{E}}_{(\boldsymbol{x},y)\sim\mathcal{S}_f^-}[\mathbb{1}(f(\boldsymbol{x}_{\mathsf{rev}})\neq f(\boldsymbol{x}))]\\ =&\mathop{\mathbb{E}}_{(\boldsymbol{x},y)\sim\mathcal{D}}[\mathbb{1}(f(\boldsymbol{x})=y)\cdot\mathbb{1}(f(\boldsymbol{x}_{\mathsf{adv}})\neq y)]+\mathop{\mathbb{E}}_{(\boldsymbol{x},y)\sim\mathcal{D}}[\mathbb{1}(f(\boldsymbol{x})\neq y)\cdot\mathbb{1}(f(\boldsymbol{x}_{\mathsf{rev}})\neq f(\boldsymbol{x}))]\\ =&\mathop{\mathbb{E}}_{(\boldsymbol{x},y)\sim\mathcal{D}}\left[\mathbb{1}(f(\boldsymbol{x})=y)\cdot\max_{\boldsymbol{x}'\in\mathcal{B}_\epsilon(\boldsymbol{x})}\mathbb{1}(f(\boldsymbol{x}')\neq y)\right]\\ &+\mathop{\mathbb{E}}_{(\boldsymbol{x},y)\sim\mathcal{D}}\left[\mathbb{1}(f(\boldsymbol{x})\neq y)\cdot\max_{\boldsymbol{x}'\in\mathcal{B}_\epsilon(\boldsymbol{x})}\mathbb{1}(f(\boldsymbol{x}')\neq f(\boldsymbol{x}))\right]\\ =&\mathop{\mathbb{E}}_{(\boldsymbol{x},y)\sim\mathcal{D}}\left[\mathbb{1}(f(\boldsymbol{x})=y)\cdot\max_{\boldsymbol{x}'\in\mathcal{B}_\epsilon(\boldsymbol{x})}\mathbb{1}(f(\boldsymbol{x}')\neq f(\boldsymbol{x}))\right]\\ &+\mathop{\mathbb{E}}_{(\boldsymbol{x},y)\sim\mathcal{D}}\left[\mathbb{1}(f(\boldsymbol{x})\neq y)\cdot\max_{\boldsymbol{x}'\in\mathcal{B}_\epsilon(\boldsymbol{x})}\mathbb{1}(f(\boldsymbol{x}')\neq f(\boldsymbol{x}))\right]\\ =&\mathop{\mathbb{E}}_{(\boldsymbol{x},y)\sim\mathcal{D}}\left[\max_{\boldsymbol{x}'\in\mathcal{B}_\epsilon(\boldsymbol{x})}\mathbb{1}(f(\boldsymbol{x}')\neq f(\boldsymbol{x}))\right]\\ =&\mathop{\mathbb{E}}_{(\boldsymbol{x},y)\sim\mathcal{D}}[\mathbb{1}(f(\boldsymbol{x}_{\mathsf{rev}})\neq f(\boldsymbol{x}))]\end{aligned}$$

□

C Additional Discussions

We showed that correctly classified examples (hypocritical examples) could be easily found in the vicinity of misclassified clean examples. As a result, a hypocritically perturbed set could be constructed with these hypocritical examples. The victim model's standard accuracy evaluated on the hypocritically perturbed set becomes higher than that on the clean set. It is natural then to wonder: *How about adversarially robust accuracy (i.e., accuracy under adversarial perturbations) of the victim model on hypocritical examples?* It's easy to see that, if the adversary is bounded by the same ϵ ball as the false friend, the model's adversarial accuracy evaluated on hypocritically perturbed set is zero, since a misclassified example exists in the ϵ ball of a hypocritical example (by definition). However, if the adversary's power is restricted by another δ ball such that $\delta<\epsilon$, then a robust hypocritical example may exist in the vicinity of a clean example so that a δ-bounded adversary can not change the model's prediction on the robust hypocritical example. In such a case, the model's adversarial accuracy evaluated on the robustly hypocritically perturbed set could be higher than that on the clean set. New attack and defense methods are required to explore this phenomenon.